Journal Name

ARTICLE

Hierarchical Nanowire Arrays Based on Carbon Nanotubes and Co_3O_4 decorated ZnO for Enhanced Photoelectrochemical Water Oxidation

Received 00th January 20xx,
Accepted 00th January 20xx

DOI: 10.1039/x0xx00000x

www.rsc.org/

Mu Li,[ab] Kun Chang,[b] Tao Wang,[b] Lequan Liu,[c] Huabin Zhang,[b] Peng Li,*[b] and Jinhua Ye*[abc]

A highly enhanced activity for photoelctrochemical water splitting was achieved by fabricating a carbon nanotube (CNT) and Co_3O_4 decorated hierarchical ZnO nanowire (NW) arrays via a facile stepwise synthesis strategy. The ternary CNTs-ZnO-Co_3O_4 NWs composite exhibits an increased photocurrent density (1.9 mA cm^{-2} at 0.6 V vs. Ag/AgCl, 2.7 times larger than the pristine ZnO NWs), improved incident photon to current conversion efficiency (52.5% at 340 nm, 5.1 times higher than the pristine ZnO NWs) as photoanode under AM 1.5G simulated sunlight. This enhancement is attributed to the specific heterogeneous ternary architecture, which evolved a promoted electron-hole charge separation and transfer, decreased water oxidation overpotential as well as increased reaction rates of water splitting by decorating ZnO NWs with CNTs and Co_3O_4.

Introduction

Since steadily worsening environmental pollution and energy shortages have raised awareness of a potential global crisis, the development of both pollution-free technologies for environmental remediation and alternative clean energy supplies became an urgent task in the past decade.[1-5] Photoelectrochemical (PEC) water splitting appears as a promising way to capture and store the solar energy as well as to produce renewable clean energy by simulating the natural photocatalysis process.[6-9] Between the two half reactions of water splitting, water oxidation reaction possess a specific status. Because it is not only the half reaction of water splitting, but also the anodic reaction of liquid phase reduction of CO_2, which would dominate the total activities. In this regard, it is still a challenging target for preparation photoanodes using cost-effective semiconductor materials with high energy conversion efficiency.

Semiconductor nanowires (NWs) have been studied extensively for over two decades for their promising electronic, photonic, thermal, electrochemical and mechanical properties.[10, 11] It is possible to achieve a large-scale implementation of solar-to-fuel energy conversion by taking the advantages of nanowire materials, such as large surface area, reduced electrochemical overpotential, enhanced light absorption and improved charge collection. In particular, ZnO nanowires with tunable alignment and morphology have been attracting great deal of attention due to their prospective electronic and optical properties. Additionally, the typical electron mobility in ZnO is 10–100 times higher than that in TiO_2, so the electrical resistance is much lower and the electron-transfer efficiency is higher than TiO_2.[12-18] Despite great efforts have been reported for the synthesis and application of ZnO NWs arrays, there is still some drawbacks accompanied by ZnO photocatalyts, such as the photocorrosion induced by photogenerated holes and the slow interfacial kinetics for water splitting.[19-21] Thus, it is highly desirable to improve the photogenerated charges separation and accelerate the reaction rates of water oxidation. The integration of photo-absorbing substrate with effective charge conductor materials appears a favorable way to overcome these disadvantages and enhance the efficiency of PEC water splitting. The hierarchical nanostructure would benefit the PEC water splitting by reducing the external power consumption, depressing the photogenerated charge recombination and facilitating the interface charge transfer.[22-26] Co_3O_4 bears the responsibility of efficient O_2 evolution and long durability against chemical- and photo-corrosion, and has been widely employed as low cost catalyst or cocatalyst for robust water oxidation in electrochemical and PEC water splitting.[27-31] Besides, Carbon nanotubes (CNTs) possess unique electrical and optical properties that make them an ideal candidate for charge separation, transport, and collection in photovoltaics due to their conspicuous merits in improving the photoconversion efficiency.[32-34]

Herein, we report a facile design and fabrication of hierarchical nanowire arrays based on CNTs and Co_3O_4

[a]*Graduate School of Chemical Science and Engineering, Hokkaido University, Sapporo 060-0814 (Japan) E-mail: Jinhua.YE@nims.go.jp*
[b]Environmental Remediation Materials Unit and International Center for Materials Nanoarchitectonics (WPI-MANA), National Institute for Materials Science 1-1 Namiki, Tsukuba, Ibaraki 305-0044 (Japan) Li.Peng@nims.go.jp
[c]TU-NIMS Joint Research Center, School of Materials Science and, Engineering, Tianjin University, 92 Weijin Road, Tianjin (P.R. China)
† Electronic Supplementary Information (ESI) available. See
DOI: 10.1039/x0xx00000x

decorated ZnO via a stepwise preparation process including chemical soaking and electrosynthesis method. Different amount of CNTs and Co_3O_4 have been loaded on ZnO NWs arrays substrate by finely controlling the concentration of CNTs aqueous solutions as well as the electrodeposition time inside the cobalt precursor electrolyte. The ternary nanostructured CNTs-ZnO-CO_3O_4 NWs arrays demonstrated obviously enhanced PEC water splitting performance, i.e. enhanced photocurrent density (1.9 mA cm-2 at 0.6 V vs. Ag/AgCl) and stability , comparing with the binary CNTs-ZnO, Co_3O_4-ZnO NWs and the pristine ZnO NWs arrays. This is attributed to the successful charge separation within the hierarchical nanostructure, increased total conductivity induced by the loaded CNTs and the excellent water oxidation behavior of decorated Co_3O_4 as cocatalysts. By introducing CNTs into the ZnO NWs arrays to fabricate interlaced structure and increase the total conductivity, the electron-hole separation from ZnO to CNTs has been highly strengthened. Meanwhile, integration with the efficient holes transfer from ZnO to Co_3O_4, a superior PEC water splitting performance was achieved. This work provides a simple fabrication of hierarchical CNTs-ZnO-Co_3O_4 NWs arrays as efficient photoanode materials to improve the PEC water splitting performance by facilitating the photogenerated charge separation and transfer efficiency.

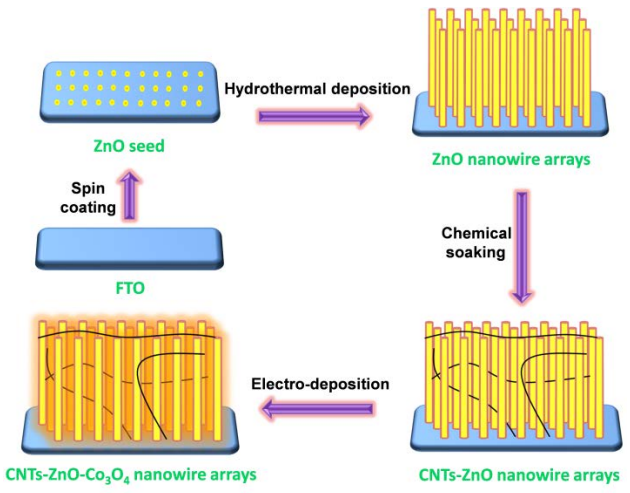

Figure 1. Schemaic illustration of the synthesis route of the hierarchical CNTs and Co_3O_4 decorated ZnO NWs arrays.

Results and Discussion

The synthesis process of ternary CNTs and Co_3O_4 decorated ZnO NWs arrays composite on fluorine-doped tin oxide (FTO) substrate is illustrated in Figure 1. Firstly, a layer of ZnO seeds was distributed on FTO substrate. The ZnO NWs were prepared via a hydrothermal process by referring the method reported in literature[15]. Then, the obtained ZnO NWs were soaked in CNTs aqueous solution to form the interlaced structure with ZnO NWs. The CNTs powders were treated with 3:1 H_2SO_4/HNO_3 mixture for functionalization and better dispersion in water before use.[35] The as-prepared CNTs-ZnO NWs were decorated with cobalt precursor via an electrosynthesis route and subsequently annealed in air. Finally, the ternary CNTs and Co_3O_4 decorated ZnO NWs arrays were obtained.

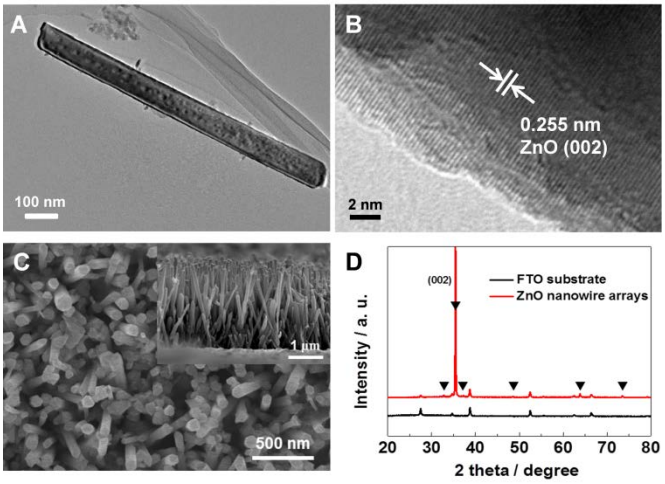

Figure 2. (A) TEM image, (B) HRTEM image, (C) SEM image (inset: cross section) and (D) XRD pattern of ZnO NWs arrays (marked by ▼)

The crystal structures and microstructures of the prepared ZnO NWs were examined by X-ray diffraction (XRD), scanning electron microscope (SEM) and transmission electron microscopy (TEM) as shown in Figure 2. The ZnO NWs were vertically aligned on the FTO substrate with an average diameter of ~ 90 nm. The length of the ZnO NWs is about 2 μm as cross section view shown in the inset of Figure 2C. Figure 2D exhibits the XRD patterns of FTO substrate and ZnO/FTO, respectively. The main peak at 2θ value of 35.1° can be indexed to (002) crystal phase, which confirms the preferential anisotropic growth along the [001] direction of FTO. This anisotropic growth is further identified by HRTEM image in Figure 2B. The microscopic morphologies of ZnO NWs prepared in different hydrothermal synthesis conditions are shown in Figure S1. Different concentrations of CNTs aqueous solution were adopted to integrate with ZnO NWs in order to optimize the amount of CNTs. The SEM images (Figure S2) finely confirm that ZnO NWs and CNTs interlaced with one another. Time-dependent experiments were carried out to study the formation process of Co_3O_4 on the hierarchical NWs arrays. Figure 3 exhibits the SEM images of the ternary CNTs and Co_3O_4 decorated ZnO NWs arrays with different electrosynthesis time. When the deposition time is 10s, only a small amount of nanoflake Co_3O_4 subunits were loaded on the surface of ZnO NWs (Figure 3A and 3B). As the electrodeposition time was prolonged gradually, the Co_3O_4 nanoflakes grow bigger and more densely (30s: Figure 3C and 3D; 50s: Figure 3E and 3F). After the electrosynthesis duration is extented to 70s, the ZnO NWs are fully wrapped with the Co_3O_4 nanoflakes (Figure S3). In particular, the nanostructure has changed to core-shell nanoarrays. UV-vis absorption spectra of the ternary CNTs and Co_3O_4 decorated ZnO NWs arrays with various electrodeposition durations are shown in

Figure S4. The spectra exhibit similar absorption properties with intense absorption edges. With the deposition time increasing, some absorption peaks appear in the visible light region due to the visible light response of Co_3O_4.[36]

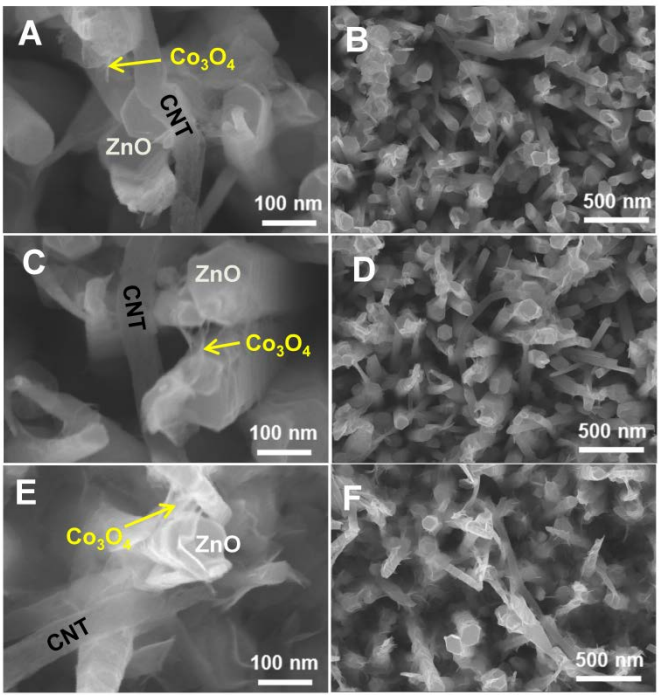

Figure 3. SEM images of the ternary CNTs and Co_3O_4 decorated ZnO NWs arrays with various electrodeposition time: (A), (B) 10s; (C), (D) 30s; (E), (F) 50s.

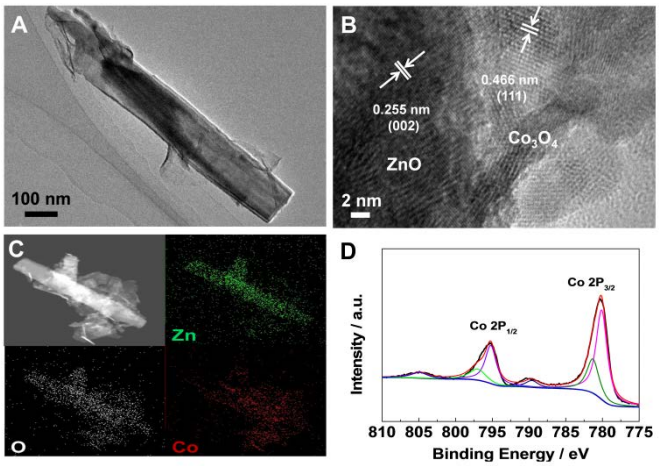

Figure 4. (A) TEM image, (B) HRTEM image, (C) EDX mapping and (D) XPS spectra of Co 2p for the CNTs and Co_3O_4 decorated ZnO NWs.

The detailed microscopic morphology and nanostructure information of the ternary CNTs-ZnO-CO_3O_4 NWs arrays were further investigated by HRTEM, EDX and XPS as shown in Figure 4. The TEM image shows the specific nanoflake-like Co_3O_4 decorated ZnO NWs morphology (Figure 4A), which is in accordance well with the SEM results. ZnO NWs and Co_3O_4 nanoflakes can be clearly distinguished in the HRTEM image (Figure 4B), and it also indicate a finely contacted interface. The corresponding EDX mapping analysis (Figure 4C) confirms that zinc is located in the central part of the NWs while cobalt is homogeneously distributed around the NWs. In order to confirm the phase state of the cobalt oxide, the ternary NWs arrays sample is characterized by XPS analysts (Figure 4D). The Co 2*p* XPS spectra show two major peaks with binding energy values at 795.1 and 780.1 eV, corresponding to the Co $2p_{1/2}$ and Co $2p_{3/2}$ spin–orbit peaks of the Co_3O_4 phase, respectively. The Co 2*p* peaks can be decomposed to Co^{3+} and Co^{2+} oxidation state, with Co^{3+} presenting a more dominant state. The weak satellite structure is ascribed to a shake-up related to the Co^{2+} component of the structure.[37] It is clearly detected in the spectrum that a satellite peak at 790.3 eV is about 9 eV higher than the position of the main peak of Co $2p_{3/2}$. This is associated with the typical assignment of cobalt oxidation states in Co_3O_4.[38] Thus, it can be deduced that the electrodeposited cobalt precursors have successfully been converted to Co_3O_4 after annealing in air.

The photoelectrocatalytic performance of the pristine ZnO NWs, binary CNTs-ZnO NWs, Co_3O_4-ZnO NWs and the ternary CNTs-ZnO-Co_3O_4 NWs arrays as photoanodes were investigated in PEC water splitting under AM 1.5G light. All the current-voltage results were recorded in a 0.5 M Na_2SO_4 (pH 6.8) aqueous solution with the potential region from -0.2 V to 1.2 V vs. Ag/AgCl at a scan rate of 10 mV s^{-1}. The pristine ZnO NWs were synthesized in various concentrations of zinc nitrite solutions during the hydrothermal process to optimize the preparation conditions of ZnO NWs. The corresponding photocurrent densities are shown in Figure S5. The best PEC performance is observed at the ZnO NWs prepared in 0.06 M zinc nitrite aqueous solution, where the current density exceeded 0.7 mA cm^{-2} at 0.6 V (approximate to 1.23 V vs. RHE). It is mainly attributed to a better growth of crystal and space alignment in this 0.06 M zinc nitrite solution. Thus, the ZnO NWs used in the following study are all synthesized in this condition. The PEC performances of the binary CNTs-ZnO NWs synthesized in different concentration of CNTs aqueous solutions are shown in Figure S6. The samples prepared in 0.25 mg mL^{-1} and 0.50 mg mL^{-1} CNTs aqueous solutions show obvious enhancement of the photocurrent densities, especially in the potential region of 0.0 V to 0.6 V. It can be deduced that the CNTs interlaced with the ZnO NWs increase the total conductivity of the binary CNTs-ZnO NWs arrays. However, with the concentration of CNTs aqueous solution increased to 1.00 mg mL^{-1}, the photocurrent density decreases dramatically. It is mainly because that too many CNTs loaded on ZnO NWs block the light as shown in Figure S2G and S2F. As the sample prepared in 0.25 mg mL^{-1} CNTs aqueous solution exhibited the best PEC performance, this 0.25 mg mL^{-1} CNTs aqueous solution was adapted for the following synthesis of the ternary CNTs and Co_3O_4 decorated ZnO NWs arrays. The binary Co_3O_4 decorated ZnO NWs arrays were also synthesized as contrast samples. The morphology exhibits the same growth tendency as the ternary NWs arrays. With increasing the deposition time of the cobalt precursor, Co_3O_4 nanoflakes grow more densely as show in Figure S7. The corresponding PEC performances are shown in Figure S8. The photocurrent densities show a

pronounced enhancement compared with the pristine ZnO NWs. Co_3O_4-ZnO (30s) exhibits the best activity, where the current density increases to ca. 1.3 mA cm^{-2} at 0.6 V under illumination.

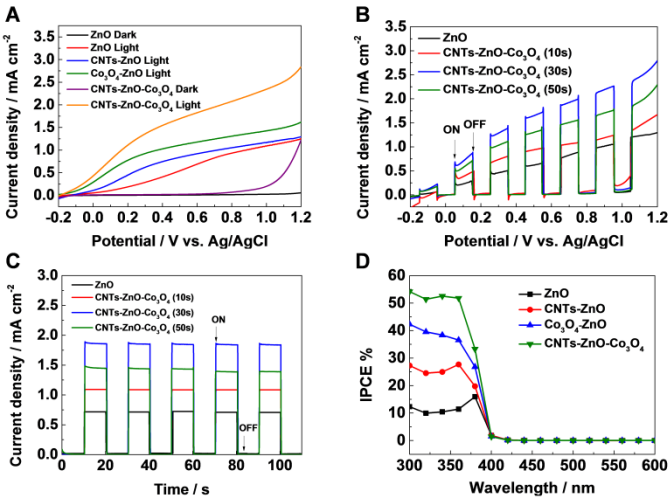

Figure 5. (A) Current-voltage curves of pristine ZnO NWs, binary CNTs-ZnO (0.25 mg mL-1) NWs, Co_3O_4-ZnO (30 s) NWs and ternary CNTs-ZnO-Co_3O_4 (30 s) NWs; (B) current-voltage curves of pristine ZnO NWs and ternary CNTs-ZnO-Co_3O_4 NWs under chopped light illumination; (C) amperometric I-t curves of pristine ZnO NWs and ternary CNTs-ZnO-Co_3O_4 NWs measured at 0.6V; (D) IPCE spectra of pristine ZnO NWs, binary CNTs-ZnO NWs, Co_3O_4-ZnO NWs and ternary CNTs-ZnO-Co_3O_4 NWs at 0.6 V vs. Ag/AgCl.

The hierarchical CNTs-ZnO-Co_3O_4 nanoarrays were subsequently investigated as photoanodes, which exhibit promising photoelectrocatalytic activities in PEC water splitting as shown in Figure5. Figure 5A shows the comparison with the pristine ZnO NWs, binary CNTs-ZnO NWs and Co_3O_4-ZnO NWs. Both of the dark and light current densities enhanced remarkably and the photocurrent density of CNTs-ZnO-Co_3O_4 nanoarrays increased significantly in the potential region from -0.2 V to 1.2 V vs. Ag/AgCl. The photoelectric response of CNTs-ZnO-Co_3O_4 nanoarrays photoanode starts at a more negative onset potential, and the photocurrent density roaringly increases to 1.9 mA cm^{-2} at 0.6 V under illumination. It is about 2.7 times larger than that of pristine ZnO NWs as well as 1.9 times and 1.5 times larger than the binary CNTs-ZnO NWs and Co_3O_4-ZnO NWs at 0.6 V, respectively. These results indicate that the PEC performance for water splitting was definitely enhanced by decorating the ZnO NWs with CNTs and Co_3O_4 to form the hierarchical nanostructure. Additionally, the cathodic shift of the onset potential suggests that a decreased charge recombination and a reduced overpotential in the ternary nanoarrays photoanode.[9, 19]

In order to further investigate the effect of the Co_3O_4 decorated on the CNTs-ZnO NWs, the photocurrent densities of the ternary composites with various cobalt precursor deposition time were carried out during repeated ON-OFF illumination cycles. As shown in Figure 5B, a steady and prompt photoresponse can be observed. The measured photocurrents are greatly affected by the loading amount of Co_3O_4. The ternary nanoarrays photoanode reaches the maximum activity when the cobalt precursor deposition time is 30s. With the deposition time exceeding this proper level, the photocurrent decreases significantly. A dense wrapping up of the Co_3O_4 nanoflakes seems to have hindered the light absorption. Moreover, densely loaded Co_3O_4 resulted in more contact of Co_3O_4 with CNTs, increases the recombination between the electrons in CNTs and the holes in Co_3O_4, so that the charge transfer efficiency within the composite has been deceased obviously. Thus, the loading of Co_3O_4 should be controlled in an optimal amount, not only to fully realize its ability as cocatalysts for water oxidation but also to avoid its contact with CNTs as well as the corresponding charge recombination. The transient photocurrents of the samples were examined during the light ON-OFF cycling at 0.6 V as shown in Figure 5C. All of the samples exhibit prompt and reproducible photocurrent responses upon each illumination. It further confirms that the photogenerated charges have promptly transferred from ZnO NWs to the loaded CNTs and Co_3O_4. Thus, this ternary hierarchical nanostructure effectively enhances the optical pathway and assists the charge separation. When comparing our photocurrent density as photoanode with the commonly reported ZnO,[19, 39-42] TiO_2,[43-46] Fe_2O_3,[47-49] WO_3[50, 51] based photoelectrodes in the literatures (usually around 1 mA cm^{-2} at ~1.2 V vs. RHE), the results in this work exhibits superior PEC activity. This can be attributed to the facilitated charge transfer and increased water splitting reaction rates by forming the ternary CNTs and Co_3O_4 decorated ZnO NWs arrays composites nanostructure.

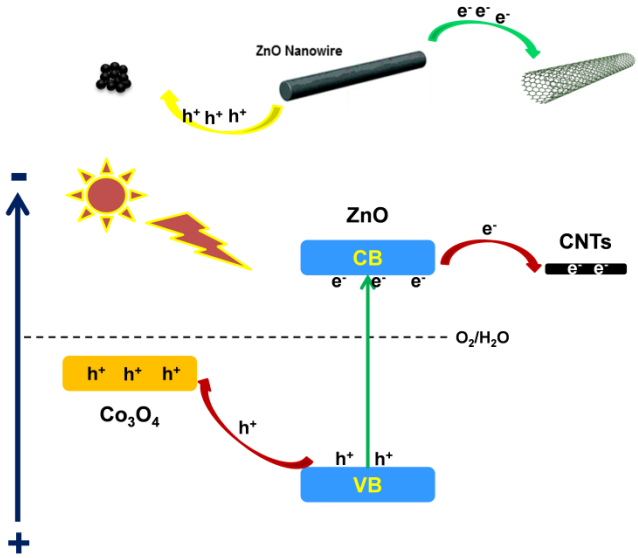

Figure 6. Schematic illustration of the charge transfer in ternary CNTs-ZnO-Co_3O_4 NWs arrays under illumination.

Incident photon to current conversion efficiency (IPCE) was evaluated at 0.6 V vs. Ag/AgCl for the pristine ZnO NWs, binary CNTs-ZnO NWs, Co_3O_4-ZnO NWs and the ternary CNTs-ZnO-Co_3O_4 NWs arrays, in order to understand the interplay between the photoactivity and light absorption as shown in

Figure 5D. IPCE can be expressed as IPCE = 1240 $j_p(\lambda)$ / $\lambda E_\lambda(\lambda)$, where $j_p(\lambda)$ is the measured photocurrent density (mA cm^{-2}), λ is the incident light wavelength (nm) and $E_\lambda(\lambda)$ is the incident monochromatic light power density (mW cm^{-2}) at a specific wavelength. The photocurrent responses of the binary and ternary NWs arrays exhibit almost the same feature as the absorption spectrum of pristine ZnO NWs, suggesting that the observed photocurrent is mainly based on the band gap transition of ZnO. The ternary CNTs-ZnO-Co_3O_4 NWs arrays exhibit significant enhancement of photoactivity. It shows the highest IPCE value of 52.5% at 340 nm, which is 5.1 times higher than that of the pristine ZnO NWs as well as 2.1 times and 1.4 times higher than the binary CNTs-ZnO NWs and Co_3O_4-ZnO NWs, respectively.

Electrochemical impedance spectroscopy (EIS) was carried out to further confirm the advantage of the ternary CNTs-ZnO-Co_3O_4 NWs in improving the charge transfer (Figure S9). A smaller size of the semicircle arc diameters indicates a more effective separation of the photogenerated electron-hole pair and a faster interfacial charge transfer to the electron donor acceptor.[52, 53] The charge separation and transfer abilities are in the order of CNTs-ZnO-Co_3O_4 NWs > CNTs-ZnO NWs > Co_3O_4-ZnO NWs > ZnO NWs. Both of the decorated CNTs and Co_3O_4 have exhibited effective ability in improving the charge transfer. Although using oxygen-containing groups to functionalize CNTs would reduce the length and conductivity of CNTs,[54, 55] the charge transfer resistance has been effectively reduced by loading CNTs on ZnO NWs. Figure 6 illustrates a supposed schematic model of the charge transfer pathway in the ternary CNTs-ZnO-Co_3O_4 NWs arrays under illumination. CNTs facilitate the charge separation and transfer by increasing the conductivity of the nanoarrays in a macroscopic aspect. In a microscopic point of view, since not each ZnO nanowire possess the same conductivity, only the high-conductivity nanowire could timely transfer the photogenerated electron to the FTO substrate before recombination. After interlacing the ZnO NWs with CNTs, CNTs bridge the low-conductivity nanowire, high-conductivity nanowire and FTO substrate together. Thus, the electron generated in the low-conductivity nanowire could also be timely transferred to the FTO substrate through CNTs and high-conductivity nanowire mediately under bias. On the other hand, Co_3O_4, as an effective water oxidation cocatalyst,[27, 28, 56] could further promote the charge separation and transfer from ZnO to Co_3O_4. Thus the recombination of photogenerated hole-electron pairs has been decreased. Moreover, the chemical stability of CNTs-ZnO-Co_3O_4 NWs has also been improved due to the promoted holes transfer from ZnO to Co_3O_4, which can prevent ZnO from photo-corrosion. As shown in Figure S10, the photocurrent response is almost identical over 30 cycles. In addition, Co_3O_4 is also an effective material in decreasing water oxidation overpotential and increasing reaction rates of water splitting. It is usually associated with the mechanism involving the electrochemical steps of Co(II) → Co(III) and Co(III) → Co(IV).[56, 57] Therefore, accounting for the synergistic cooperation of CNTs and Co_3O_4 in charge separation, the hierarchical construction of ternary CNTs-ZnO-Co_3O_4 NWs arrays composites demonstrates an efficient way in water splitting as a photoanode.

Conclusions

In summary, hierarchically CNTs and Co_3O_4 decorated ZnO nanowire arrays with ternary heteroassembly nanostructures have been successfully fabricated via a facile stepwise synthesis process. Detailly, CNTs were interlaced with ZnO NWs to improve the conductivity and Co_3O_4 was loaded on ZnO as water oxidation cocatalysts. ZnO NWs serves as the main photosensitizer while CNTs could act as a cocatalyst to further promote the separation and transfer of photogenerated electrons, meanwhile Co_3O_4 could synergistically transfer the holes from ZnO. Therefore, the ternary CNTs-ZnO-Co_3O_4 NWs arrays exhibit significantly enhanced activity in PEC water splitting compared with the pristine ZnO NWs, binary CNTs-ZnO NWs and Co_3O_4-ZnO NWs as photoanodes under AM 1.5G simulated sunlight. This can be attributed to the effectively improved photogenerated charge separation and transfer as well as the markedly accelerated water splitting reaction rates due to the specific ternary architecture. In addition, this facile hierarchical synthesis strategy could be extended to fabricate other semiconductor heterogeneous assemblies to achieve a sustainable and affordable solar energy conversion.

Experimental

Preparation

(I) Fabrication of ZnO NWs. ZnO NWs were prepared by a facile hydrothermal synthesis process by referring to the previous report.[15] Briefly, 100 mL of a 0.06 M solution of zinc acetate in absolute ethanol was prepared with ultrasonic agitation as seeds solution. The seeds solution was spin-coated on the pre-treated FTO substrates, and then annealed at 350 °C for 30 min to yield a layer of ZnO seeds. The seeded substrates were suspended vertically in a Teflon vessel, and then sealed in an autoclave and heated to 110 °C for 24 h for nanowire growth. The concentration of the reagent solution varies from 0.04 M to 0.07 M zinc nitrate and hexamethylenetetramine (HMT) aqueous solution to optimize the preparation condition. Finally, the nanowire substrate was removed from the autoclave, washed thoroughly with distilled water, dried in air and annealed at 300 °C for 3h in air.

(II) Fabrication of CNTs-ZnO NWs. The binary CNTs-ZnO Nws were obtained by soaking the as-prepared ZnO NWs in CNTs aqueous solution (concentration of 0.25 mg mL^{-1}, 0.50 mg mL-1 and 1.00 mg mL^{-1}). CNTs powders (Multi-walled, 40~70 nm, Wako) were treated with 3:1 H_2SO_4/HNO_3 mixture for functionalization and better dispersion in water before use.[35] The ZnO/FTO substrates were immersed in the CNTs aqueous solution for 30s, died in air and annealed at 300 °C for 3h in air.

(III) Fabrication of CNTs-ZnO-Co_3O_4 NWs. The as-obtained CNTs-ZnO/FTO substrates were subsequently used as the working electrode and placed in an electrochemical cell which

was assembled in a three-electrode configuration, by using platinum as the counter electrode and Ag/AgCl as the reference electrode. The electrodeposition of cobalt precursors were carried out by galvanostatic deposition at a current density of 1 mA cm^{-2} in 0.15 M $Co(NO_3)_2$ aqueous solution. Finally, the resulting nanowire arrays were withdrawn, rinsed with distilled water and annealed at 300 °C for 3h in air. Co_3O_4-ZnO NWs were synthesized as the same way without decorating the CNTs.

Characterization

The crystal structure of ZnO NWs was determined with an X-ray diffractometer (X'Pert Powder, PANalytical B.V., Netherlands) with Cu-Kα radiation. Scanning electron microscopy images were recorded with a HITACHI S-4800 field emission scanning electron microscopy. Transmission electron microscopy images were recorded with a field emission transmission electron microscope (2100F, JEOL Co., Japan) operated at 200 kV, combined with energy dispersive X-ray spectroscopy (EDX) for the determination of metal composition. The diffuse reflection spectra were measured with an integrating sphere equipped UV–visible recording spectrophotometer (UV-2600, Shimadzu Co., Japan) using BaSO4 as reference and the optical absorptions were converted from the reflection spectra according to Kubelka-Munk equation. Photoelectron Spectroscopy (XPS) experiments were performed in type Theta probe (Thermo Fisher Co., USA) using monochromatized Al Kα at hν = 1486.6 eV and the peak positions were internally referenced to the C 1s peak at 284.6 eV.

Photoelectrochemical Experiments

PEC activity measurements were performed with a CHI electrochemical analyser (ALS/CH model 650A) using a standard three-electrode mode with 0.5 M Na_2SO_4 (pH 6.8) solution as the electrolyte using Ag/AgCl (saturated KCl) as the reference electrode and a Pt sheet as the counter electrode. The pristine ZnO NWs, binary CNTs-ZnO NWs, Co_3O_4-ZnO NWs and the ternary CNTs-ZnO-Co_3O_4 NWs arrays were fabricated respectively as photoanode. The simulated sunlight was obtained by an AM 1.5 solar simulator (WXS-80C-3 AM 1.5G) with a light intensity of 100 mW cm^{-2}. Linear sweep voltammetry (LSV) was performed with a voltage scan speed of 10 mV s^{-1} and the light was chopped manually at regular intervals. The incident photon to electron conversion efficiency (IPCE) was calculated from chronoamperometry measurements using a motorized monochrometer (M10; Jasco Corp.). Electrochemical impedance spectroscopy (EIS) was performed at similar conditions as described above for photoelectrochemical tests. The amplitude of the sinusoidal wave was 5 mV and the frequency range examined was 100 kHz to 1 Hz.

Acknowledgements

This work was partly supported by World Premier International Research Center (WPI) Initiative on Materials Nanoarchitectonics (MANA), MEXT, Japan and National Basic Research Program of China (973 Program, 2014CB239301). M. Li gratelfully acknowledge financial support from China Scholarship Council (CSC).

References

1. H. Tong, S. Ouyang, Y. Bi, N. Umezawa, M. Oshikiri and J. Ye, *Adv. Mater.*, 2012, 24, 229-251.
2. A. Heller, *Science*, 1984, 223, 1141-1148.
3. N. S. Lewis, *Science*, 2007, 315, 798-801.
4. B. C. H. Steele and A. Heinzel, *Nature*, 2001, 414, 345-352.
5. Z. Zou, J. Ye, K. Sayama and H. Arakawa, *Nature*, 2001, 414, 625-627.
6. M. Gratzel, *Nature*, 2001, 414, 338-344.
7. A. Fujishima and K. Honda, *Nature*, 1972, 238, 37-38.
8. M. G. Walter, E. L. Warren, J. R. McKone, S. W. Boettcher, Q. Mi, E. A. Santori and N. S. Lewis, *Chem. Rev.*, 2010, 110, 6446-6473.
9. Y. Hou, F. Zuo, A. Dagg and P. Feng, *Angew. Chem. Int. Ed.*, 2013, 52, 1248-1252.
10. N. P. Dasgupta, J. Sun, C. Liu, S. Brittman, S. C. Andrews, J. Lim, H. Gao, R. Yan and P. Yang, *Adv. Mater.*, 2014, 26, 2137-2184.
11. Y. Xia, P. Yang, Y. Sun, Y. Wu, B. Mayers, B. Gates, Y. Yin, F. Kim and H. Yan, *Adv. Mater.*, 2003, 15, 353-389.
12. Z. L. Wang and J. Song, *Science*, 2006, 312, 242-246.
13. H. Yu, Z. Zhang, M. Han, X. Hao and F. Zhu, *J. Am. Chem. Soc.*, 2005, 127, 2378-2379.
14. L. Vayssieres, *Adv. Mater.*, 2003, 15, 464-466.
15. H. M. Chen, C. K. Chen, Y.-C. Chang, C.-W. Tsai, R.-S. Liu, S.-F. Hu, W.-S. Chang and K.-H. Chen, *Angew. Chem. Int. Ed.*, 2010, 49, 5966-5969.
16. A. Menzel, K. Subannajui, F. Güder, D. Moser, O. Paul and M. Zacharias, *Adv. Funct. Mater.*, 2011, 21, 4342-4348.
17. T. Wang, Z. Jiao, T. Chen, Y. Li, W. Ren, S. Lin, G. Lu, J. Ye and Y. Bi, *Nanoscale*, 2013, 5, 7552-7557.
18. T. Wang, B. Jin, Z. Jiao, G. Lu, J. Ye and Y. Bi, *J. Mater. Chem. A*, 2014, 2, 15553-15559.
19. M. Shao, F. Ning, M. Wei, D. G. Evans and X. Duan, *Adv. Funct. Mater.*, 2014, 24, 580-586.
20. C. Han, Z. Chen, N. Zhang, J. C. Colmenares and Y.-J. Xu, *Adv. Funct. Mater.*, 2014, DOI: 10.1002/adfm.201402443, n/a-n/a.
21. S. K. Karuturi, J. Luo, C. Cheng, L. Liu, L. T. Su, A. I. Y. Tok and H. J. Fan, *Adv. Mater.*, 2012, 24, 4157-4162.
22. A. Kudo and Y. Miseki, *Chem. Soc. Rev.*, 2009, 38, 253-278.
23. T. Hisatomi, J. Kubota and K. Domen, *Chem. Soc. Rev.*, 2014, 43, 7520-7535.
24. K. Maeda and K. Domen, *J. Phys. Chem. Lett.*, 2010, 1, 2655-2661.
25. J. Yang, D. Wang, H. Han and C. Li, *Acc. Chem. Res.*, 2013, 46, 1900-1909.
26. Y. Ma, X. Wang, Y. Jia, X. Chen, H. Han and C. Li, *Chem. Rev.*, 2014, 114, 9987-10043.
27. M. Liao, J. Feng, W. Luo, Z. Wang, J. Zhang, Z. Li, T. Yu and Z. Zou, *Adv. Funct. Mater.*, 2012, 22, 3066-3074.
28. L. Xi, P. D. Tran, S. Y. Chiam, P. S. Bassi, W. F. Mak, H. K. Mulmudi, S. K. Batabyal, J. Barber, J. S. C. Loo and L. H. Wong, *J. Phys. Chem. C*, 2012, 116, 13884-13889.
29. T. Y. Ma, S. Dai, M. Jaroniec and S. Z. Qiao, *J. Am. Chem. Soc.*, 2014, 136, 13925-13931.
30. N. Kang, J. H. Park, M. Jin, N. Park, S. M. Lee, H. J. Kim, J. M. Kim and S. U. Son, *J. Am. Chem. Soc.*, 2013, 135, 19115-19118.

31. J. Wang and F. E. Osterloh, *J. Mater. Chem. A*, 2014, 2, 9405-9411.
32. J. Wei, Y. Jia, Q. Shu, Z. Gu, K. Wang, D. Zhuang, G. Zhang, Z. Wang, J. Luo, A. Cao and D. Wu, *Nano Lett.*, 2007, 7, 2317-2321.
33. Z. Li, V. P. Kunets, V. Saini, Y. Xu, E. Dervishi, G. J. Salamo, A. R. Biris and A. S. Biris, *ACS Nano*, 2009, 3, 1407-1414.
34. Z. Li, S. A. Kulkarni, P. P. Boix, E. Shi, A. Cao, K. Fu, S. K. Batabyal, J. Zhang, Q. Xiong, L. H. Wong, N. Mathews and S. G. Mhaisalkar, *ACS Nano*, 2014, 8, 6797-6804.
35. Y.-C. Tsai, S.-C. Li and S.-W. Liao, *Biosens. Bioelectron.*, 2006, 22, 495-500.
36. T. Warang, N. Patel, R. Fernandes, N. Bazzanella and A. Miotello, *Appl. Catal., B*, 2013, 132–133, 204-211.
37. N. S. McIntyre, D. D. Johnston, L. L. Coatsworth, R. D. Davidson and J. R. Brown, *Surf. Interface Anal.*, 1990, 15, 265-272.
38. Y. Wang, Z.-W. Fu and Q.-Z. Qin, *Thin Solid Films*, 2003, 441, 19-24.
39. K. Pan, Y. Dong, W. Zhou, Q. Pan, Y. Xie, T. Xie, G. Tian and G. Wang, *ACS Appl. Mater. Interfaces*, 2013, 5, 8314-8320.
40. X. Yang, A. Wolcott, G. Wang, A. Sobo, R. C. Fitzmorris, F. Qian, J. Z. Zhang and Y. Li, *Nano Lett.*, 2009, 9, 2331-2336.
41. M. Zhong, Y. Li, I. Yamada and J.-J. Delaunay, *Nanoscale*, 2012, 4, 1509-1514.
42. Y.-G. Lin, Y.-K. Hsu, Y.-C. Chen, L.-C. Chen, S.-Y. Chen and K.-H. Chen, *Nanoscale*, 2012, 4, 6515-6519.
43. A. Wolcott, W. A. Smith, T. R. Kuykendall, Y. Zhao and J. Z. Zhang, *Small*, 2009, 5, 104-111.
44. J. Cao, Y. Zhang, H. Tong, P. Li, T. Kako and J. Ye, *Chem. Commun.*, 2012, 48, 8649-8651.
45. Q. Kang, J. Cao, Y. Zhang, L. Liu, H. Xu and J. Ye, *J. Mater. Chem. A*, 2013, 1, 5766-5774.
46. S. Hoang, S. Guo, N. T. Hahn, A. J. Bard and C. B. Mullins, *Nano Lett.*, 2011, 12, 26-32.
47. D. K. Zhong and D. R. Gamelin, *J. Am. Chem. Soc.*, 2010, 132, 4202-4207.
48. K. J. McDonald and K.-S. Choi, *Chem. Mat.*, 2011, 23, 1686-1693.
49. J. Cao, L. Liu, A. Hashimoto and J. Ye, *Electrochem. Commun.*, 2014, 48, 17-20.
50. D.-D. Qin, C.-L. Tao, S. A. Friesen, T.-H. Wang, O. K. Varghese, N.-Z. Bao, Z.-Y. Yang, T. E. Mallouk and C. A. Grimes, *Chem. Commun.*, 2012, 48, 729-731.
51. X. Chen, J. Ye, S. Ouyang, T. Kako, Z. Li and Z. Zou, *ACS Nano*, 2011, 5, 4310-4318.
52. W. H. Leng, Z. Zhang, J. Q. Zhang and C. N. Cao, *J. Phys. Chem. B*, 2005, 109, 15008-15023.
53. X. F. Cheng, W. H. Leng, D. P. Liu, Y. M. Xu, J. Q. Zhang and C. N. Cao, *J. Phys. Chem. C*, 2008, 112, 8725-8734.
54. Y. Zhang, J. Li, Y. Shen, M. Wang and J. Li, *J. Phys. Chem. B*, 2004, 108, 15343-15346.
55. Y. Shen, J. S. Reparaz, M. R. Wagner, A. Hoffmann, C. Thomsen, J.-O. Lee, S. Heeg, B. Hatting, S. Reich, A. Saeki, S. Seki, K. Yoshida, S. S. Babu, H. Mohwald and T. Nakanishi, *Chem. Sci.*, 2011, 2, 2243-2250.
56. M. Barroso, A. J. Cowan, S. R. Pendlebury, M. Grätzel, D. R. Klug and J. R. Durrant, *J. Am. Chem. Soc.*, 2011, 133, 14868-14871.
57. J. A. Koza, Z. He, A. S. Miller and J. A. Switzer, *Chem. Mat.*, 2012, 24, 3567-3573.